Morphology, Crystallization, and Thermal Behavior of Isotactic Polypropylene/Polymethylmethacrylate Blends: Effects of the Addition of a Graft Copolymer of Propylene with Methylmethacrylate

L. D'ORAZIO,[1] R. GUARINO,[1] C. MANCARELLA,[1] E. MARTUSCELLI,[1] G. CECCHIN[2]

[1] Istituto di Ricerca e Tecnologia delle Materie Plastiche del CNR Via Toiano, 6, 80072 Arco Felice, Napoli, Italy

[2] Montell Italia S.p.A, Ferrara, Italy

Received 3 December 1999; accepted 28 March 2000

ABSTRACT: Optical microscopy, differential scanning calorimetry, and small angle X-ray scattering techniques were used to study the influence of crystallization conditions on the morphology and thermal behavior of samples of ternary blends constituted of isotactic polypropylene (iPP), atactic polymethylmethacrylate (aPMMA), and a novel graft copolymer of unsaturated propylene with methylmethacrylate (uPP-*g*-PMMA). The purpose was to assess the uPP-*g*-PMMA capability to act as compatibilizer for iPP/aPMMA materials. It was shown that the presence of uPP-*g*-PMMA copolymer affects the interfacial tension between the iPP and aPMMA phase in the melt state, the aPMMA particle size, and particle-size distribution is modified. After complete crystallization of the iPP phase at relatively low undercooling, in a range of crystallization temperatures, the presence of the uPP-*g*-PMMA phase was found to modify both mode and state of dispersion of minor component and spherulitic texture and inner structure of spherulites fibrillae. The extent of the induced modifications was dependent on a combination of composition and undercooling. Also, relevant thermodynamic parameters of the iPP phase, such as the equilibrium melting temperature and the surface free energy of folding, were strongly affected by the presence of the uPP-*g*-PMMA phase, opposite effects being observed depending on the uPP-*g*-PMMA content. The observed melting temperature and surface free energy of folding values were accounted for by the growth of iPP lamellar crystals with different perfection, thickness, and surface disorder. © 2000 John Wiley & Sons, Inc. J Appl Polym Sci 79: 143–158, 2001

Key words: polypropylene; propylene-*g*-methylmethacrylate; polymethylmethacrylate; morphology; crystallization

INTRODUCTION

A novel graft copolymer of unsaturated propylene with methylmethacrylate (uPP-*g*-PMMA) was added to binary blends of isotactic polypropylene (iPP) and atactic polymethylmethacrylate (aPMMA) to assess whether such a copolymer can be used for compatibilizing iPP/aPMMA materials. In previous work[1] dealing with solution-cast samples, it was shown that, contrary to expectation, the uPP-*g*-PMMA addition does not provide iPP/aPMMA compatibilized materials irrespective of composition, even though the crystalline texture of the iPP matrix was strongly modified.

Correspondence to: L. D'Orazio.

Journal of Applied Polymer Science, Vol. 79, 143–158 (2001)
© 2000 John Wiley & Sons, Inc.

Table I Molecular Characteristics of the Starting Polymers Together with Glass Transition Temperature (T_g), Apparent Melting Temperature (T'_m), and Crystallinity Index (X_c)

Sample	$\bar{M}_n$ (g/mol)	$\bar{M}_w$ (g/mol)	$\bar{M}_w/\bar{M}_n$	η (dL/g)	% PMMA (wt/wt)	T_g (°C)	T'_m (°C)	X_c
iPP	78,700	509,000	6.5	2.0	—	7	164	0.47
aPMMA	—	116,000	—	—	—	134	—	—
uPP-*g*-PMMA	—	—	—	1.3	20	23	141	0.28

As a matter of fact, the degree of dispersion of the minor component achieved, following the addition of uPP-g-PMMA copolymer, remained comparable to that exhibited by binary blends of iPP and aPMMA with no relevant evidence of adhesion or interconnection between the phases. However, because of the copolymer presence, with increasing uPP-*g*-PMMA content (wt/wt), the iPP spherulites were found to become more open and coarse and the dimensions and number per unit area of the amorphous interspherulitic contact regions were found to increase. Accordingly, the copolymer uncrystallizable sequences were assumed to be located mainly in interfibrillar and interspherulitic amorphous contact regions. Small angle X-ray scattering (SAXS) analysis demonstrated that the phase structure developed in the iPP/aPMMA/uPP-*g*-PMMA blends was characterized by values of the long period increasing linearly with increasing copolymer content (wt/wt). Assuming a two-phase model for the iPP spherulite fibrillae, constituted by alternating parallel crystalline lamellae and amorphous layers, the lamellar structure of the iPP phase in the ternary blends was characterized by crystalline lamellar thickness (L_c) and interlamellar amorphous layer (L_a) higher than that shown by plain iPP, and L_c and L_a values, which both increased with increasing uPP-*g*-PMMA content (wt/wt). Such SAXS results were accounted for by assuming that a cocrystallization phenomenon between propylenic sequences of the uPP-*g*-PMMA copolymer and iPP occurred. The development of the iPP lamellar structure in the iPP/aPMMA/uPP-*g*-PMMA blends was thus modeled hypothesizing that during such a cocrystallization process, copolymer PMMA chains with comparatively lower molecular mass, remain entrapped in the iPP interlamellar amorphous layer, forming their own domains. Moreover, evidence of strong correlations between the crystallization process of the uPP-*g*-PMMA copolymer and the iPP crystallization process was shown also by differential scanning calorimetry (DSC) and wide angle X-ray scattering experiments.

In this article, we report on the results of studies aimed at establishing the influence of the crystallization conditions on the morphology of the phase and interphase developed after complete iPP crystallization from the melt state under controlled crystallization conditions. Film samples of binary iPP/PMMA and ternary iPP/PMMA/uPP-*g*-PMMA blends isothermally crystallized, at a relatively low undercooling in a range of crystallization temperatures of the iPP phase, were thus prepared. The combined effect of undercooling and composition on the kinetic and thermodynamic parameters related to the isothermal crystallization process of the iPP phase also have been investigated.

EXPERIMENTAL

The starting polymers used in this study were iPP (HS005) made by Himont, aPMMA, made by BDH Chemicals Ltd. (Poole-Dorset, UK), and an uPP-*g*-PMMA copolymer synthesized in the Himont Scientific Laboratories according to methods patented by Cecchin et al.[2,3] from Himont. The molecular characteristics of the iPP, aPMMA, and uPP-*g*-PMMA samples are reported in Table I.

Blending and Sample Preparation

All the investigated samples were obtained by means of the solvent casting method. The blend components were dissolved in a common solvent, *o*-dichlorobenzene, at a total polymer concentration of 3% by weight and at the temperature of 135°C. Thin films were then obtained by *o*-dichlorobenzene casting performed under vacuum at a temperature of 135°C for 3 h. iPP/aPMMA (80:20 wt/wt) binary blends and iPP/aPMMA/uPP-*g*-

PMMA ternary blends containing 2, 5, and 10% (wt/wt) of graft copolymer were prepared.

Techniques

DSC

The thermal behavior of the thin films of plain iPP, binary, and ternary blends isothermally crystallized at the temperatures of 126, 130, 134, and 138°C was analyzed by means of DSC with a Mettler TA 3000 instrument equipped with a control and programming unit (microprocessor Tc 10). The apparent melting temperatures (T'_m) and the crystallinity indices (X_c) were determined following this procedure: the film samples (about 9 mg) were heated from room temperature up to 200°C with a rate of 10°C/min and kept at this temperature for 10 min to destroy any trace of crystallinity, then were rapidly cooled to desired crystallization temperature (T_c); after complete crystallization, such samples were again heated to 200°C at a rate of 10°C /min. The observed melting temperatures (T'_m) and the apparent enthalpies of melting (ΔH^*) were obtained from the maxima and the area of the melting peaks, respectively. The crystallinity indexes (X_c) of iPP and of blends were calculated by applying the following relations:

$$X_c(\text{iPP}) = \Delta H^*(\text{iPP})/\Delta H^0(\text{iPP}) \quad (1)$$

$$X_c(\text{blend}) = \Delta H^*(\text{blend})/\Delta H^0(\text{iPP}) \quad (2)$$

where ΔH^*(iPP) is the apparent enthalpy of fusion per gram of iPP in the blend; $\Delta H°$ (iPP) is the heat of fusion per gram of 100% crystalline iPP, from (4) $\Delta H°$ (iPP) = 209 J/g, and ΔH^*(blend) is the apparent enthalpy of fusion per gram of blend. The crystalline weight fractions referred to the iPP phase in blends [X_c(iPP)] were calculated from the following relation:

$$X_c(\text{iPP}) = X_c(\text{blend})/W(\text{iPP}) \quad (3)$$

where W(iPP) is the weight fraction of iPP in the blends.

Optical Microscopy

Thin films of plain iPP, binary, and ternary blends, isothermally crystallized at the temperatures of 126, 130, 134, and 138°C according to the same procedure used to study the isothermal crystallization process of the iPP phase by DSC, were observed by means of optical microscopy. A Zeiss optical polarizing microscope fitted with a Mettler hot stage was used; optical micrographs were taken with crossed and parallel polarizers. The radial growth rates (G) of the observed iPP spherulites were calculated by measuring the spherulite size (R) as a function of time; the photomicrographs were taken on the print and G was calculated as the slope of the straight lines obtained by plotting R against the time. The Zeiss microscope was also used to observe melts of binary and ternary blends at the temperature of 200°C and kept at this temperature for 10 min.

SAXS

SAXS studies on films of plain iPP, binary, and ternary blends isothermally crystallized at the temperatures of 126, 130, 134, and 138°C were performed by means of a compact Kratky camera equipped with a Braun one-dimensional positional sensitive detector. Ni-filtered CuKα radiation generated from a Philips X-ray generator (PW 1730/10) operating at 40 KV and 30 mA, was used. The raw scattering data were corrected for parasitic scattering, absorption, and slit smearing by using Vonk's method.[5] The desmeared intensities were then Lorentz factor corrected by multiplying by s^2 ($s = 2\sin\theta/\lambda$).[6]

RESULTS AND DISCUSSION

Microscopy Studies in Melt and Solid State

Optical micrographs were taken with parallel polarizers, of thin films of binary iPP/aPMMA and ternary iPP/aPMMA/uPP-*g*-PMMA blends melted at the temperature of 200°C, and kept at this temperature for 10 min to destroy any crystallinity trace, and are reported in Figure 1. As shown, and as expected for an immiscible system, the iPP/aPMMA melt exhibits phase separation with the aPMMA component segregated in its own spherically shaped domains showing a relatively wide size distribution. By adding the uPP-*g*-PMMA copolymer, no homogeneous melts are achieved; dispersed phase domains are, in fact, observed irrespective of copolymer content in the blends (wt/wt). By visual impression, it seems that the addition of the uPP-*g*-PMMA copolymer modifies the mode and state of dispersion of the minor component. In fact, the number of particles per unit area seems to be increased; moreover, with increasing copolymer content, a population

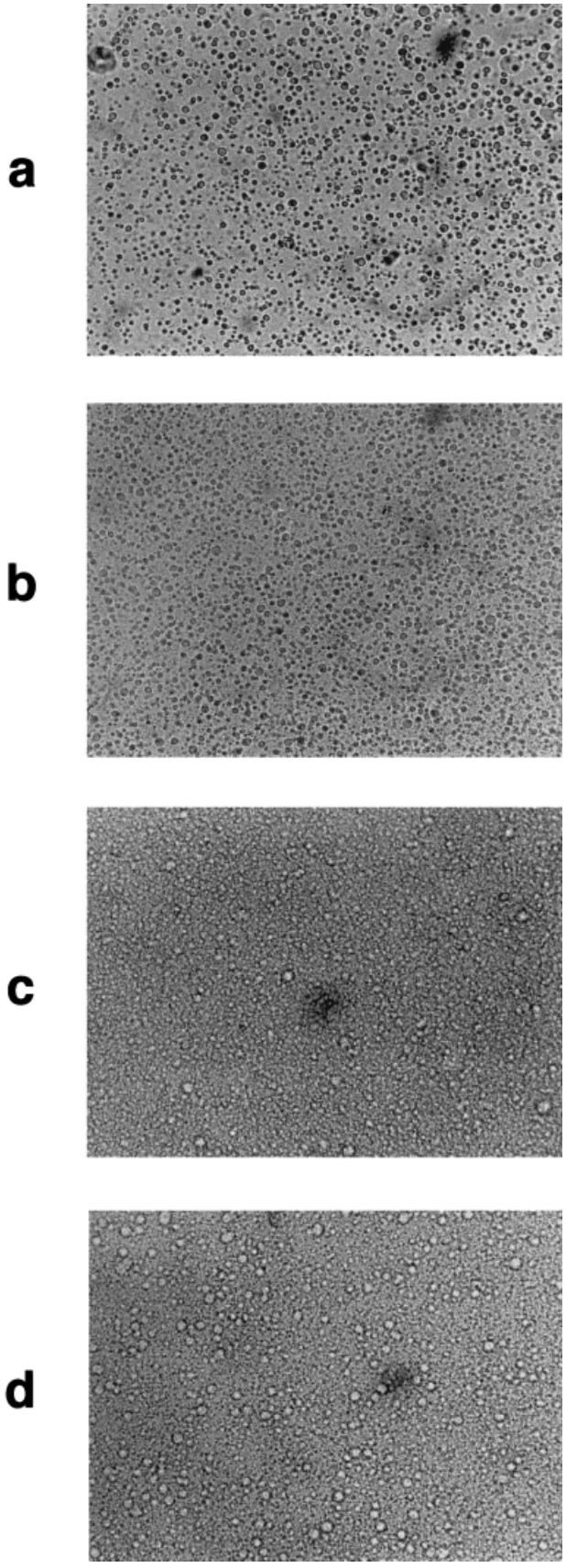

of particles with a size considerably larger than that exhibited by the aPMMA particles in the iPP/aPMMA melt, is observed (see Fig. 1). These findings indicate that the uPP-*g*-PMMA addition modifies the interfacial tension between iPP and aPMMA melts. In particular, the dispersion degree achieved indicates that the extent of the compatibilization is not essentially the same for each PMMA-based particle formed. Therefore, the above morphological results could be related to an uneven dispersion of the graft copolymer and/or different state of mixing of the uPP-*g*-PMMA copolymer with iPP and aPMMA. It should be recalled that the variation of tangent δ with the temperature for such blends, reported in previous work,[1] showed the occurrence of favorable intermolecular interactions between the copolymer propylene sequences and iPP in the amorphous condensed state.

Optical micrographs, taken at crossed and parallel polarizers of thin films of iPP/aPMMA binary and iPP/aPMMA/uPP-*g*-PMMA ternary blends isothermally crystallized at 126°C, are reported in Figure 2. For comparison, optical micrographs, taken with crossed and parallel polarizers, of thin films of plain iPP at the investigated T_c are reported in Figure 3. As shown in Figure 2, the iPP/aPMMA blend exhibits a defined spherulitic superstructure with the aPMMA phase segregated in spherical-shaped domains uniformly occluded in the iPP intra- and interspherulitic regions. Furthermore, no amorphous interspherulitic contact regions are developed; such regions are, however, shown by the plain iPP (compare Figs. 2 and 3). For a T_c of 126°C, the morphologies developed in the ternary iPP/aPMMA/uPP-*g*-PMMA blends depend on composition, that is, on uPP-*g*- PMMA content (wt/wt). The observations performed at parallel polarizers clearly show that, in the blends containing 2 and 5% (wt/wt) of uPP-*g*-PMMA copolymer, the dispersion coarseness of minor component is much finer than that developed in the iPP/aPMMA binary blends (the finest dispersion coarseness being achieved for a uPP-*g*-PS content equal to 5% wt/wt). In contrast, a wide particle size distribution, together with large and irregularly shaped domains of minor component, is observed for higher copolymer content (10%

Figure 1 Optical micrographs taken with parallel polarizers of thin films of binary iPP/aPMMA blends (a), ternary iPP/aPMMA/uPP-*g*-PMMA 2% wt/wt (b), iPP/aPMMA/uPP-*g*-PMMA 5% wt/wt (c), and iPP/aPMMA/uPP-*g*-PMMA 10% wt/wt (d) blends melted at the temperature of 200°C.

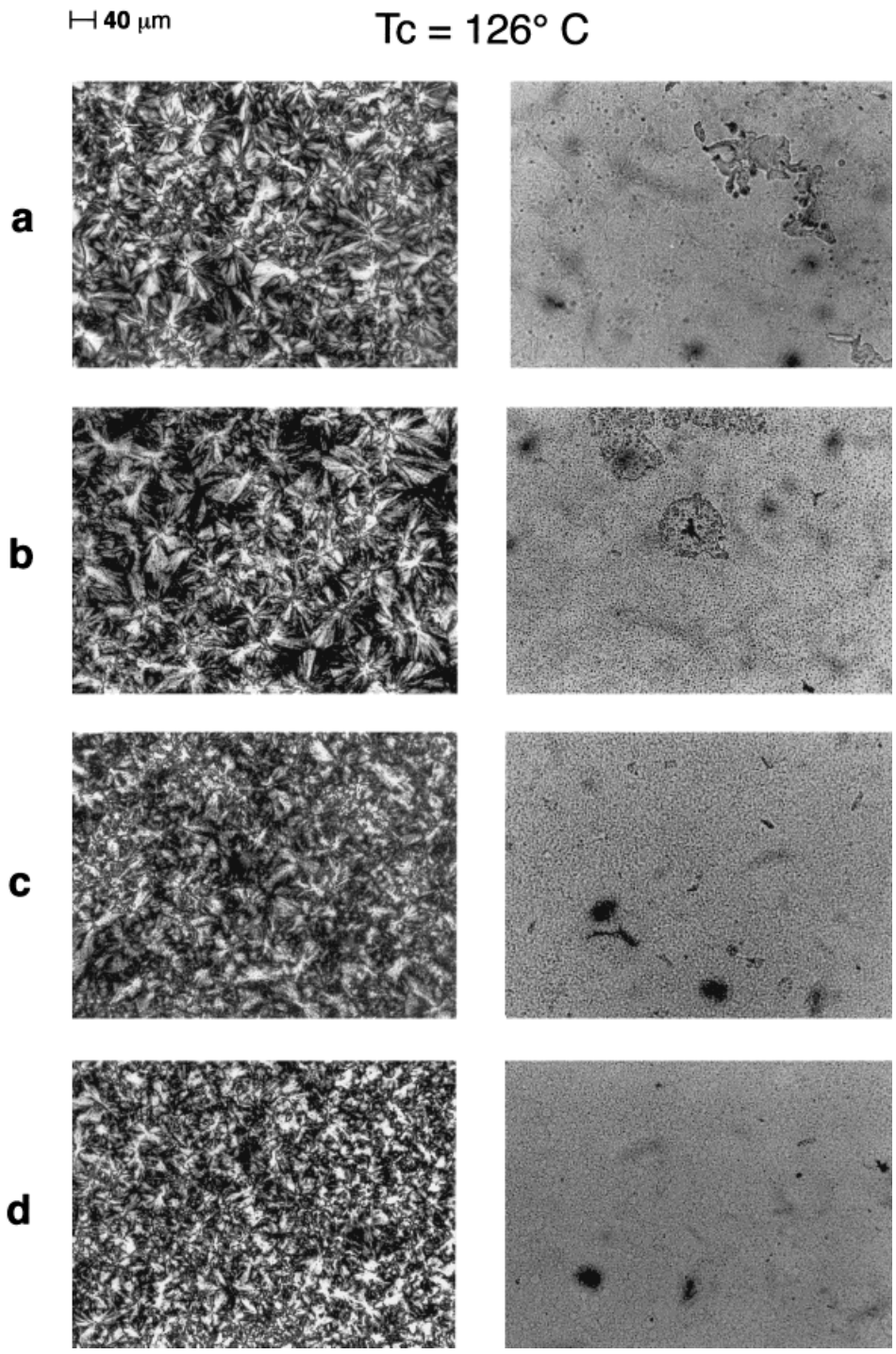

Figure 2 Optical micrographs taken with crossed and parallel polarizers of thin films of binary iPP/aPMMA blends (a), ternary iPP/aPMMA/uPP-*g*-PMMA 2% wt/wt (b), iPP/aPMMA/uPP-*g*-PMMA 5% wt/wt (c), and iPP/aPMMA/uPP-*g*-PMMA 10% wt/wt (d) blends isothermally crystallized at the temperature of 126°C.

wt/wt) (see Fig. 2). These findings suggest a compatibilization effect, following the addition of the uPP-*g*-PMMA phase, which depends on composition.

The comparison between the melt morphologies of the iPP/aPMMA/uPP-*g*-PMMA blends with the morphologies generated after iPP complete crystallization (compare Figs. 1 and 2) shows that the iPP

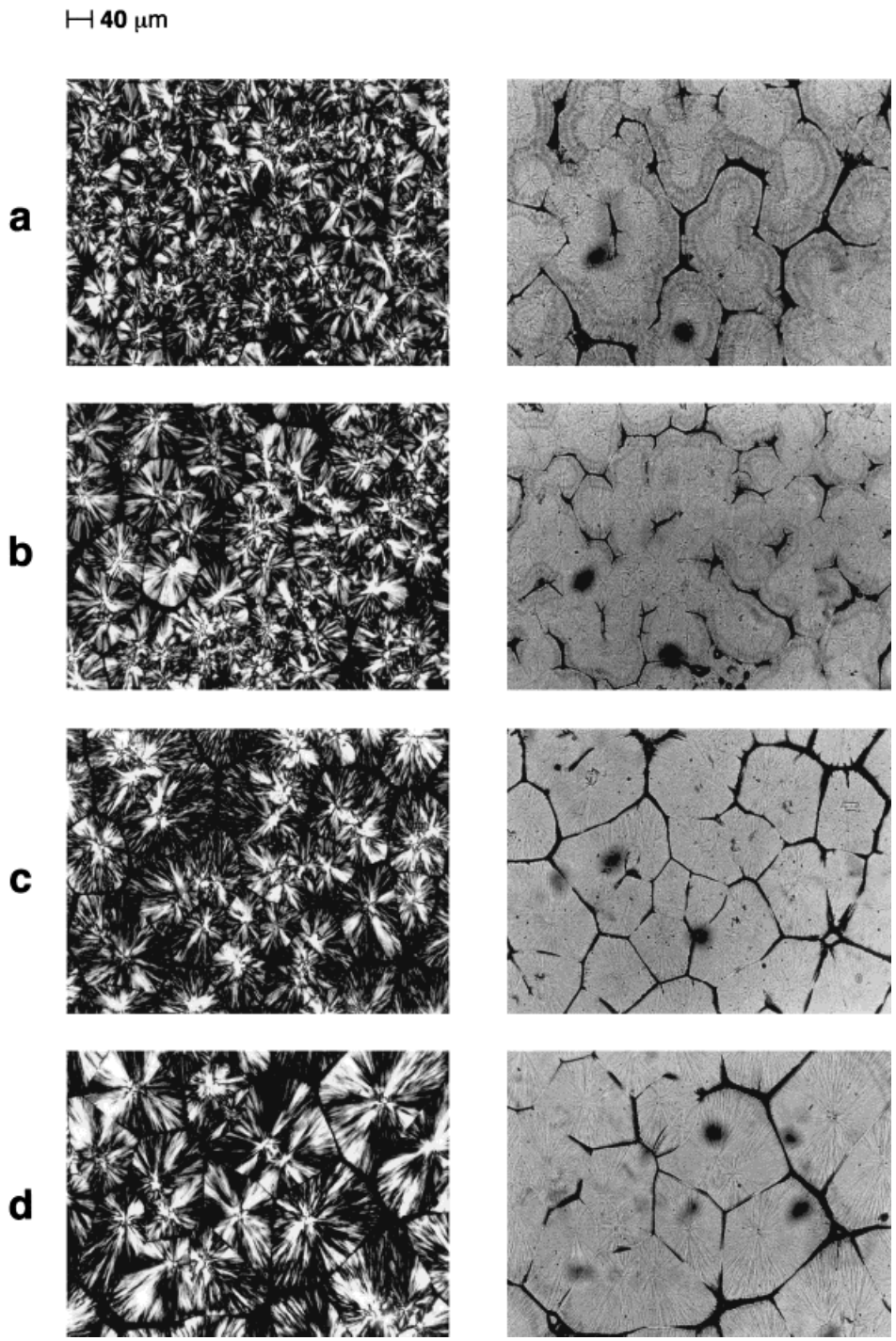

Figure 3 Optical micrographs taken with crossed and parallel polarizers of thin films of plain iPP isothermally crystallized at the temperatures of (a) 126, (b) 130, (c) 134, and (d) 138°C.

crystallization process provides interconnected materials characterized by the presence of spherulites in which neatness and regularity are damaged with increasing copolymer content. Moreover, reduced average particle size and narrowed particle-size distribution are shown by the blends containing 2 and 5% of uPP-*g*-PMMA copolymer. For the blends containing 10% of the uPP-*g*-PMMA phase, the iPP

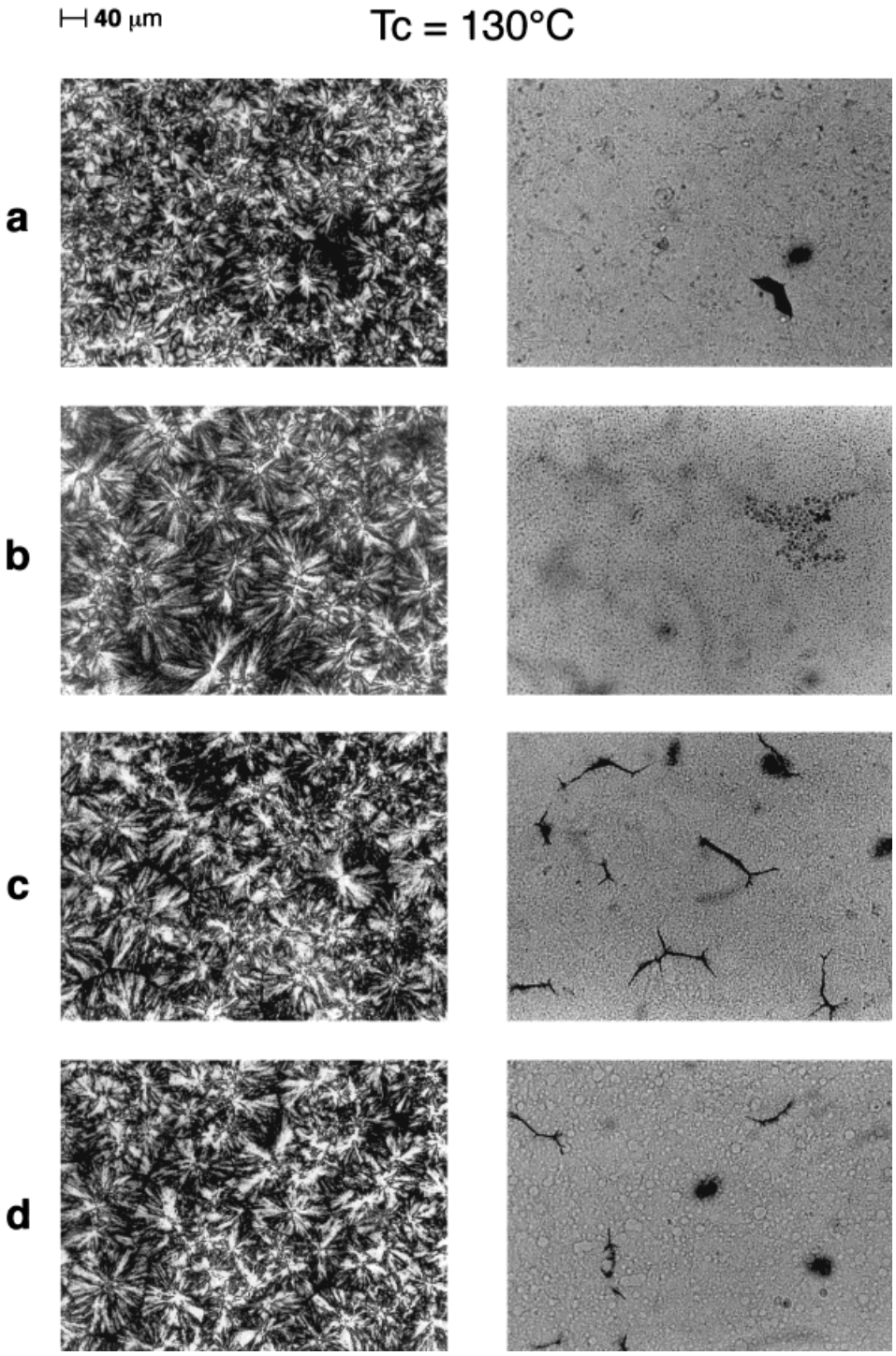

Figure 4 Optical micrographs taken with crossed and parallel polarizers of thin films of binary iPP/aPMMA blends (a), ternary iPP/aPMMA/uPP-*g*-PMMA 2% wt/wt (b), iPP/aPMMA/uPP-*g*-PMMA 5% wt/wt (c), and iPP/aPMMA/uPP-*g*-PMMA 10% wt/wt (d) blends isothermally crystallized at the temperature of 130°C.

crystallization process freezes the melt morphology of dispersed phase.

For binary iPP/aPMMA samples, a T_c of iPP phase increase of 4.0°C (130°C) induces no relevant morphological effects on both the spherulites texture and mode and state of dispersion of minor component [compare Figs. 2(a) and 4(a)], whereas for iPP/aPMMA/uPP-*g*-PMMA blends, the size of

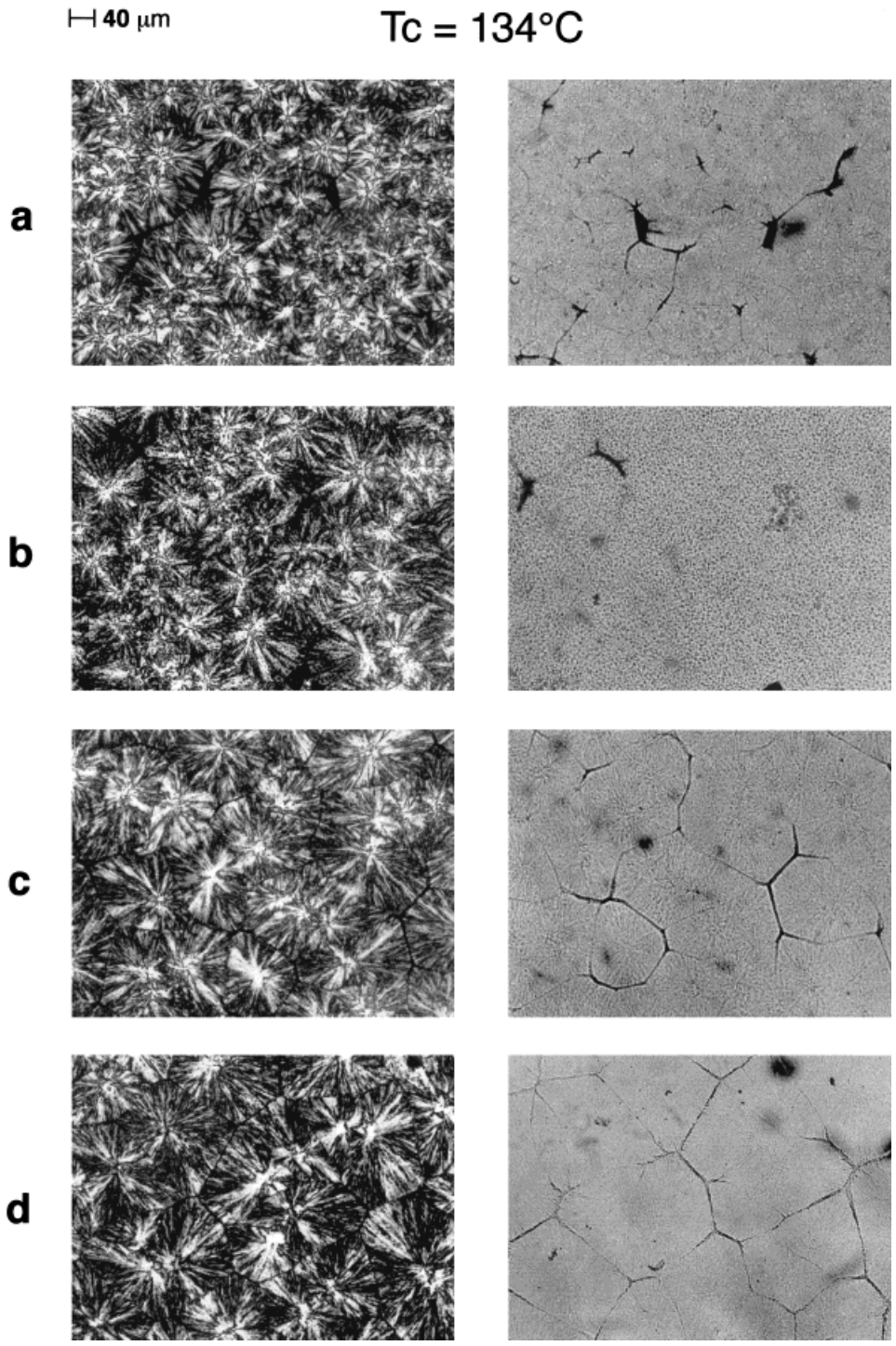

Figure 5 Optical micrographs taken with crossed and parallel polarizers of thin films of binary iPP/aPMMA blends (a), ternary iPP/aPMMA/uPP-*g*-PMMA 2% wt/wt (b), iPP/aPMMA/uPP-*g*-PMMA 5% wt/wt (c), and iPP/aPMMA/uPP-*g*-PMMA 10% wt/wt (d) blends isothermally crystallized at the temperature of 134°C.

the spherulites increases and some amorphous interspherulitic contact regions are observed [compare Fig. 2(b–d) with Fig. 4(b–d)].

By increasing T_c to 134°C, the morphology of both binary and ternary blends is strongly modified (compare Figs. 2 and 5). For the iPP/aPMMA

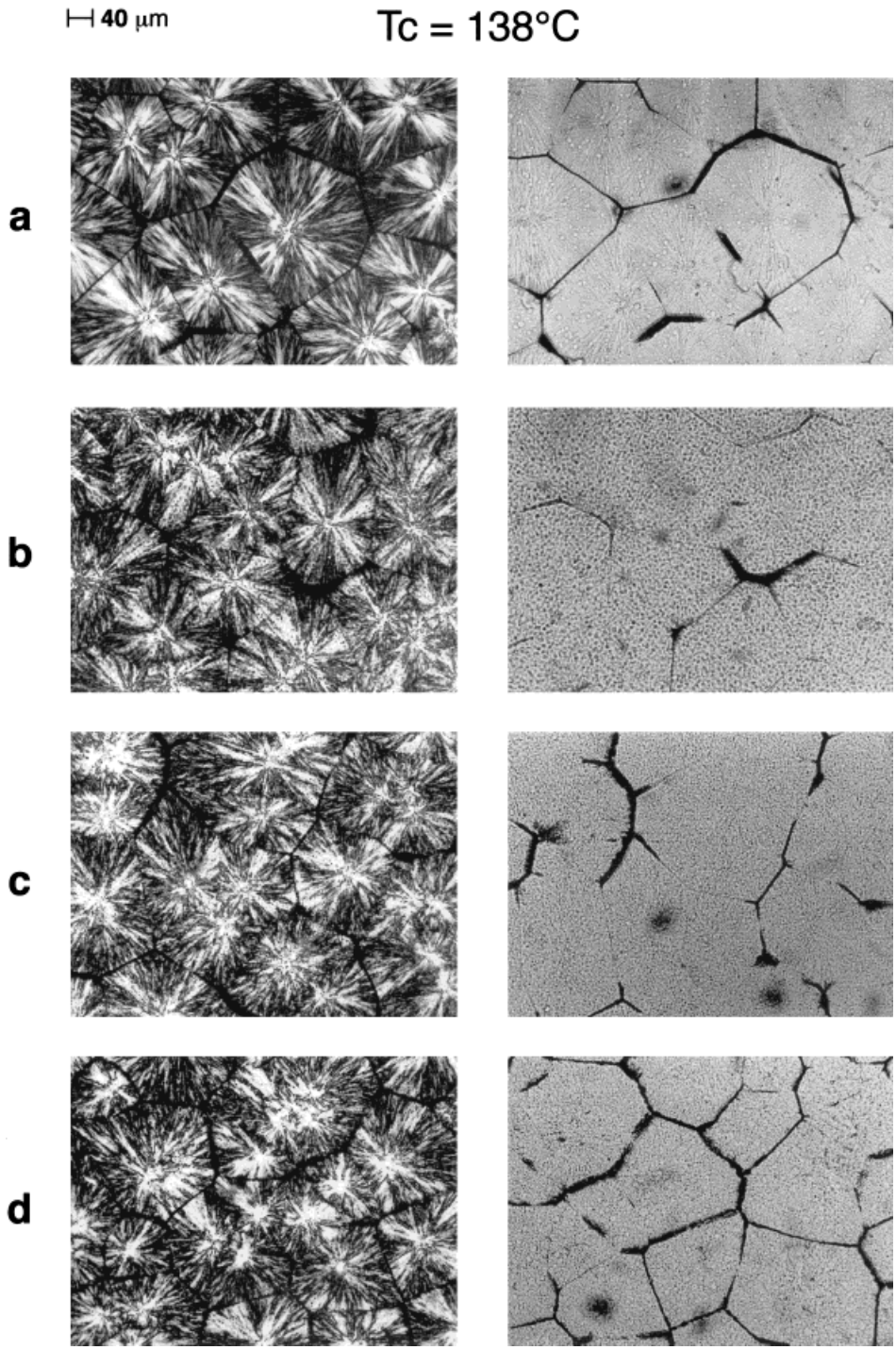

Figure 6 Optical micrographs taken with crossed and parallel polarizers of thin films of binary iPP/aPMMA blends (a), ternary iPP/aPMMA/uPP-*g*-PMMA 2% wt/wt (b), iPP/aPMMA/uPP-*g*-PMMA 5% wt/wt (c), and iPP/aPMMA/uPP-*g*-PMMA 10% wt/wt (d) blends isothermally crystallized at the temperature of 138°C.

blends, the dispersion coarseness of the aPMMA domains increases, suggesting that during the iPP crystallization process, a coalescence phenomenon is undergone by the primary particles formed in the melt state. Moreover, the spherulitic texture is characterized by the presence, al-

ready evidenced for the plain iPP at lower T_c, of amorphous interspherulitic contact regions and by spherulites showing size, neatness, and regularity slightly lower than that exhibited by spherulites of plain iPP [compare Figs.5(a) and 3(c)]. For the iPP/aPMMA/uPP-*g*-PMMA ternary blends, the increased T_c results in similar morphologies as far as the mode and state of dispersion of the minor component is concerned [see Fig. 5(b–d)]. In contrast, the neatness, regularity, and size of the spherulites of the iPP phases increase with increasing uPP-*g*-PMMA content, being higher than those shown by the iPP phase crystallized from iPP/aPMMA melts. Moreover, amorphous material seems to be rejected at the spherulitic boundary regions. Noteworthy is that, for the ternary blends containing 10% of uPP-*g*-PMMA copolymer, the dispersion coarseness, achieved by isothermally crystallizing such materials at 134°C, is noticeably lower than that developed both at lower T_c (126 and 130°C) [compare Figs. 2(d) and 4(d) with Fig. 5(d)] and in the melt state [compare Figs. 5(d) and 1(d)].

A further T_c increase (138°C) evidences, for the binary iPP/aPMMA and for the ternary blend containing 10% of copolymer, a coalescence phenomenon of the domains of dispersed phase that tend to be rejected from the crystallization front at the boundary of the spherulites and in the interspherulitic amorphous contact regions (compare Figs. 1 and 6). Moreover, the number per unit area of the amorphous interspherulitic contact regions increases with increasing uPP-*g*-PMMA content (wt/wt).

Plots of the radius of iPP spherulites, crystallized from melts of plain iPP and the binary and ternary blends against time for all the crystallization temperatures investigated, give straight lines, indicating that, irrespective of composition, the concentration of propylenic crystallizable sequences at the growth front is constant during the crystallization process. For high undercooling, the values of the radial growth rate (G) of the iPP spherulites depend on blend composition, whereas with reducing undercooling, such values are almost constant, approaching those calculated for the plain iPP (see Fig. 7). In particular for high undercooling, the spherulites of the iPP phase grown from melts of iPP/aPMMA and iPP/aPMMA/uPP-*g*-PMMA containing 2% of copolymer, and from melts of ternary blends containing 5 and 10% of uPP-*g*-PMMA phase (wt/wt), show G values respectively higher and lower than that found both for spherulites grown from melts of

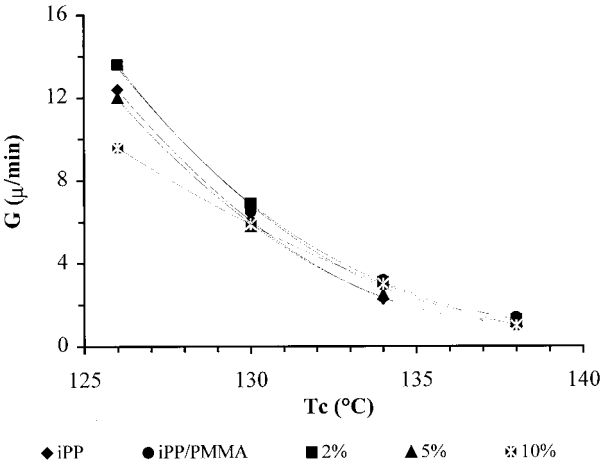

Figure 7 Plots of the radial grow rate (G) of iPP spherulites isothermally crystallized from melts of plain iPP, binary iPP/aPMMA, and ternary iPP/aPMMA/uPP-*g*-PMMA melts as a function of crystallization temperature (T_c).

plain iPP. Such findings could be accounted for by comparatively lower and higher concentration of molecular entanglements influencing the activation free energy for the transport process through the liquid–solid interface (ΔF^*), according to the well known Turnbull-Fisher equation[7] and/or by phenomena of rejection, occlusion, and deformation of dispersed domains by the growing spherulites according to Bartczak et al.[8] Insofar as the particular activation free energy for the transport process through the liquid–solid interface is concerned, one needs to take into account the problem of the conversion to surface nucleation and lamellar growth, earlier treated by Turnbull and Fisher.[7] This requires accounting for the work of chain folding, the quite different nature of the transport mechanism (reptation) in the polymer melt, the effect of chain length, the segmental nature of the polymer chain, and questions related to the substrate length and the nature of a surface nucleus on a blade-like structure.[9] It could be therefore hypothesized that, for high undercooling, the rate of transport of the iPP crystallizable sequences in the iPP/aPMMA/uPP-*g*-PMMA melts can be retarded or promoted depending on a combination of thermodynamic and kinetic effects related to the phase nature and concentration in the immediate regions of the growing lamellae and to mode and state of dispersion of the minor component in the melt state.

Table II Apparent Melting Temperatures (T'_m) for Plain iPP and iPP Crystallized from Its Blends as a Function of the Crystallization Temperature (T_c)

	T'_m (°C)			
Sample	T_c = 126°C	T_c = 130°C	T_c = 134°C	T_c = 138°C
iPP	165	166	168	170
iPP/PMMA	164	166	169	171
iPP/PMMA/uPP-*g*-PMMA, graft 2% (wt/wt)	164	165	167	170
iPP/PMMA/uPP-*g*-PMMA, graft 5% (wt/wt)	165	166	168	169
iPP/PMMA/uPP-*g*-PMMA, graft 10% (wt/wt)	166	165	167	169

DSC Studies

The thermograms of isothermally crystallized samples of plain iPP and its binary iPP/aPMMA and ternary iPP/aPMMA/uPP-*g*-PMMA blends show, for all investigated crystallization temperatures, a single endothermic peak when heated from room temperature up to 200°C. The temperatures corresponding to the maxima of such peaks (T'_m) are reported in Table II. The crystallinity indices of the blends (X_c) and of the iPP phase [X_c(iPP)] for the T_c investigated are reported in Tables III and IV, respectively. As shown in Tables II–IV, and as expected, the apparent melting temperature values and crystallinity indices of all the investigated samples tend to increase with increasing crystallization temperature. For a given T_c: the following results are remarked upon:

- The T'_m values shown by iPP phase crystallized from binary iPP/aPMMA and ternary iPP/aPMMA/uPP-*g*-PMMA blends are, within experimental error, independent of the composition; that is, such values are comparable to that exhibited by the plain iPP.
- The crystallinity indices of the iPP/aPMMA binary and iPP/aPMMA/uPP-*g*-PMMA ternary blends are considerably lower than that exhibited by the plain iPP; the extent of such a decrease becoming larger with reducing undercooling (see Table III).
- The iPP/aPMMA/uPP-*g*-PMMA ternary blends containing 2% of copolymer show X_c values comparable to that shown by the iPP/aPMMA blends, whereas X_c values considerably lower are exhibited by the ternary blends containing 5 and 10% of the uPP-*g*-PMMA phase.
- The X_c values of the iPP phase crystallized from the iPP/PMMA binary blends are close to that shown by the plain iPP, indicating that the presence in the melt state of segregated aPMMA domains (see Fig. 1) slightly interfere with the iPP crystallization process.

Table III Crystallinity Indices (X_c) of Plain iPP, iPP/PMMA, and iPP/PMMA/uPP-*g*-PMMA Blends as a Function of the Crystallization Temperature (T_c)

	X_c			
Sample	T_c = 126°C	T_c = 130°C	T_c = 134°C	T_c = 138°C
iPP	0.50	0.52	0.53	0.54
iPP/PMMA	0.40	0.41	0.40	0.42
iPP/PMMA/uPP-*g*-PMMA, graft 2% (wt/wt)	0.40	0.40	0.41	0.42
iPP/PMMA/uPP-*g*-PMMA, graft 5% (wt/wt)	0.33	0.34	0.34	0.39
iPP/PMMA/uPP-*g*-PMMA, graft 10% (wt/wt)	0.35	0.36	0.37	0.38

Table IV Crystallinity of iPP Phase as a Function of the Crystallization Temperature (T_c)

Sample	X_c(iPP)			
	T_c = 126°C	T_c = 130°C	T_c = 134°C	T_c = 138°C
iPP	0.50	0.52	0.53	0.54
iPP/PMMA	0.50	0.51	0.50	0.53
iPP/PMMA/uPP-*g*-PMMA, graft 2% (wt/wt)	0.50	0.50	0.51	0.53
iPP/PMMA/uPP-*g*-PMMA, graft 5% (wt/wt)	0.41	0.43	0.43	0.49
iPP/PMMA/uPP-*g*-PMMA, graft 10% (wt/wt)	0.44	0.45	0.46	0.48

- The X_c values of the iPP phase crystallized from the iPP/aPMMA/uPP-*g*-PMMA ternary blends depends on composition (i.e., on iPP-*g*-PMMA content). For low copolymer content (2%), such X_c values are comparable to that shown by iPP crystallized in the presence of aPMMA. With increasing uPP-*g*-PMMA content, such values noticeably decrease, indicating that the presence of uPP-*g*-PMMA phase strongly interferes with the iPP crystallization process. Such findings suggest that, irrespective of dispersion coarseness achieved in the blends, the aPMMA based particles are not easily ejected and/or occluded by the iPP crystallization front.

SAXS Studies

Typical Lorentz-corrected desmeared patterns for isothermally crystallized samples of binary iPP/aPMMA and ternary iPP/PMMA/uPP-*g*-PMMA blends are shown in Figure 8. As shown, such SAXS profiles exhibit well defined maxima. By applying Bragg's law, the long period (L) of the iPP phase has been calculated from the peak position. Assuming a two-phase model for the iPP spherulite fibrillae, consisting of alternating parallel crystalline lamellae and amorphous layers, the crystalline lamellar thickness (L_c) has been calculated using the following relation for the L values:

$$L_c = \frac{X_{c(\mathrm{iPP})} \cdot L}{(\rho_c/\rho_a)(1 - X_{c(\mathrm{iPP})}) + X_{c(\mathrm{iPP})}} \qquad (4)$$

where $X_{c(\mathrm{iPP})}$ is the DSC crystallinity index of the iPP phase and ρ_c and ρ_a are the densities of the crystalline and amorphous iPP phase, respectively. The thickness of the amorphous interlamellar layer (L_a) has been calculated by:

$$L_a = L - L_c \qquad (5)$$

The long period, lamellar thickness, and amorphous interlamellar thickness of the plain iPP and iPP crystallized from its binary and ternary blends are reported in Tables V–VII as a function of T_c. As is to be expected, for both plain iPP and iPP crystallized from binary iPP/aPMMA and ternary iPP/aPMMA/uPP-*g*-PMMA blends, L and L_c values increase with increasing crystallization temperature (see Tables V and VI). However, for a given T_c, there is no clear dependence of the L values on composition. It is interesting to observe that when, for a given T_c, iPP crystallizes in the

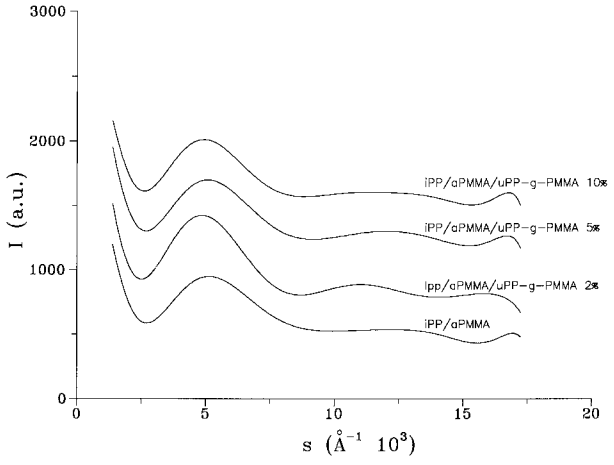

Figure 8 Typical SAXS Lorentz-corrected desmeared profiles for isothermally crystallized samples of binary iPP/aPMMA and ternary iPP/aPMMA/uPP-*g*-PMMA blends.

Table V The Long Period (L) Values for Plan iPP and iPP Crystallized from Its Blend as a Function of the Crystallization Temperature (T_c)

	L (Å)			
Sample	T_c = 126°C	T_c = 130°C	T_c = 134°C	T_c = 138°C
iPP	188	192	219	246
iPP/PMMA	175	197	219	239
iPP/PMMA/uPP-*g*-PMMA, graft 2% (wt/wt)	188	197	213	239
iPP/PMMA/uPP-*g*-PMMA, graft 5% (wt/wt)	164	183	225	246
iPP/PMMA/uPP-*g*-PMMA, graft 10% (wt/wt)	183	192	208	213

presence of aPMMA the phase structure developed in the iPP/aPMMA blends is characterized by crystalline lamellar thickness and interlamellar amorphous layer thickness comparable to that shown by plain iPP (see Tables VI and VII). Such findings confirm that the iPP crystallization process from iPP/aPMMA melts is almost unaffected by the presence of the aPMMA domains. For the iPP phase crystallized from the ternary blends, irrespective of T_c, no increase in the L values are found, thus indicating that the uPP-*g*-PMMA phase is not present between the iPP lamellae. It should be noted that the uPP-*g*-PMMA addition results in the average crystalline thickness of the iPP phase being strongly dependent on copolymer content. For an uPP-*g*-PMMA content equal to 2%, L_c values closely approach those exhibited by the iPP phase crystallized in the presence of aPMMA (see Table VI). With increasing uPP-*g*-PMMA content, the L_c values decrease noticeably (see Table VI), whereas no systematic increase in the L_a values is observed (see Table VII). Such results indicate that the uPP-*g*-PMMA phase can interfere with the iPP crystallization process, the extent of such an interference depending on composition.

By plotting the apparent melting temperature (T'_m) obtained by DSC versus the inverse of the crystalline lamellar thickness of iPP phase ($1/L_c$) straight lines can be drawn (see Fig. 9). Thus, the trend of T'_m against L_c can be described by the following relation:

$$T'_m = T_m - \frac{2\sigma_e T_m}{\Delta H_f}\frac{1}{L_c} \tag{6}$$

where T'_m is the apparent melting temperature; ΔH_f, the enthalpy of the fusion of 100% crystalline iPP; L_c, the crystalline lamellar thickness; T_m, the equilibrium melting temperature; and σ_e, the surface free energy of folding. According to this

Table VI Crystalline Lamella Thickness (L_c) Values for Plain iPP and iPP Crystallized from Its Blends as a Function of the Crystallization Temperature (T_c)

	L_c (Å)			
Sample	T_c = 126°C	T_c = 130°C	T_c = 134°C	T_c = 138°C
iPP	89	93	104	124
iPP/PMMA	83	98	111	123
iPP/PMMA/uPP-*g*-PMMA, graft 2% (wt/wt)	89	94	104	121
iPP/PMMA/uPP-*g*-PMMA, graft 5% (wt/wt)	63	74	91	115
iPP/PMMA/uPP-*g*-PMMA, graft 10% (wt/wt)	76	82	91	97

Table VII Interlamellar Amorphous Layer Thickness (L_a) Values for Plain iPP and iPP Crystallized from Its Blends as a Function of the Crystallization Temperature (T_c)

Sample	L_a (Å)			
	T_c = 126°C	T_c = 130°C	T_c = 134°C	T_c = 138°C
iPP	99	99	115	122
iPP/PMMA	92	99	108	116
iPP/PMMA/uPP-*g*-PMMA, graft 2% (wt/wt)	99	103	109	118
iPP/PMMA/uPP-*g*-PMMA, graft 5% (wt/wt)	101	109	134	131
iPP/PMMA/uPP-*g*-PMMA, graft 10% (wt/wt)	107	110	117	116

equation, T_m and σ_e can be determined, respectively, from the intercept and slope of the straight lines obtained by plotting T'_m against $1/L_c$. The T_m and σ_e values, determined by this method, are reported in Table VIII. As shown in the Table, the plain iPP shows T_m and σ_e values in line with those reported in the literature.[5] To be noted is that the iPP phase crystallized from iPP/aPMMA/uPP-*g*-PMMA melts containing low copolymer content shows both T_m and σ_e values higher than those exhibited by the iPP phase crystallized in presence of aPMMA phase and, surprisingly, by the plain iPP also. In contrast, much lower T_m and σ_e values are shown by the iPP phase in the remaining ternary blends (see Table VIII). These

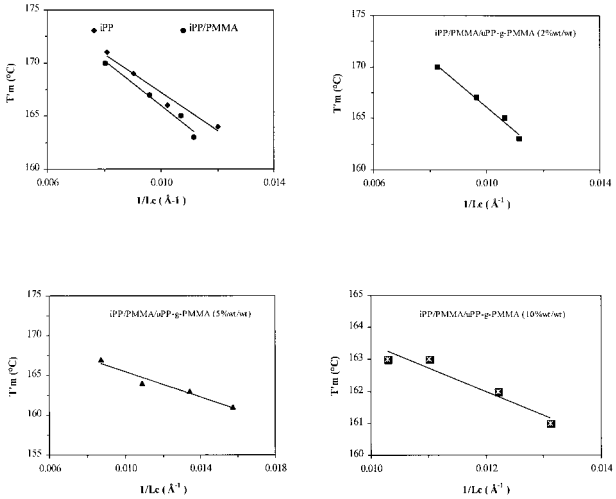

Figure 9 Plots of the apparent melting temperatures (T'_m) versus the inverse of lamellar thickness ($1/L_c$) of iPP phase isothermally crystallized from melt of plain iPP, binary iPP/aPMMA, and ternary iPP/aPMMA/uPP-*g*-PMMA melts.

results indicate that, for a given T_c, the growth of iPP crystal from its blends occurs under different undercoolings. The folding surface free energy can be expressed by the fundamental thermodynamic equation[9]:

$$\sigma_e = \Delta H_e - TS_e \tag{7}$$

where ΔH_e is the folding surface enthalpy, and S_e, the folding surface entropy. The σ_e variation can be attributed to a variation of the S_e term. Therefore, the observed changes in σ_e values are presumably attributable to an increase in the S_e term, that is, to a comparatively lower or higher surface disorder of the lamellar crystals. Plots of T_m and σ_e values of the iPP phase crystallized from its blends versus the uPP-*g*-PMMA content (wt/wt) show that there is no linear dependence of the thermodynamic parameters of iPP phase on the composition (see Figs. 10 and 11). In particu-

Table VIII Equilibrium Melting Temperature (T_m) and Surface Free Energy of Folding (σ_e) Values of Plain iPP and iPP Phase Crystallization from Its Binary and Ternary Blends

Sample	T_m (°C)	σ_e (erg/cm^2)
iPP	187	118
iPP/PMMA	185	103
iPP/PMMA/uPP-*g*-PMMA, graft 2% (wt/wt)	189	128
iPP/PMMA/uPP-*g*-PMMA, graft 5% (wt/wt)	174	48
iPP/PMMA/uPP-*g*-PMMA, graft 10% (wt/wt)	171	45

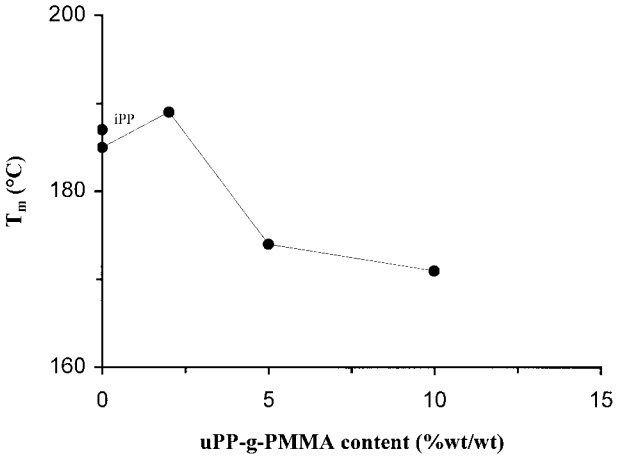

Figure 10 Plots of the equilibrium melting temperatures (T_m) of iPP phase as a function of uPP-*g*-PMMA content (wt/wt).

lar, the finding that, in the iPP/aPMMA/uPP-*g*-PMMA blends containing 2% of uPP-*g*-PMMA copolymer, the iPP crystals are characterized by the highest perfection and/or thickness and by lowest superficial disorder could be accounted for by assuming that, owing to miscibility effects between propylenic sequences of the copolymer and iPP sequences with comparatively lower regularity, the uPP-*g*-PMMA phase could extract from the iPP defective molecules, thus leaving a crystallizable phase with higher constitutional and conformational regularity. Taking into account all the above results, the lamellar structure of iPP phase developed in the ternary iPP/aPMMA/uPP-*g*-PMMA blends is compared with that generated in

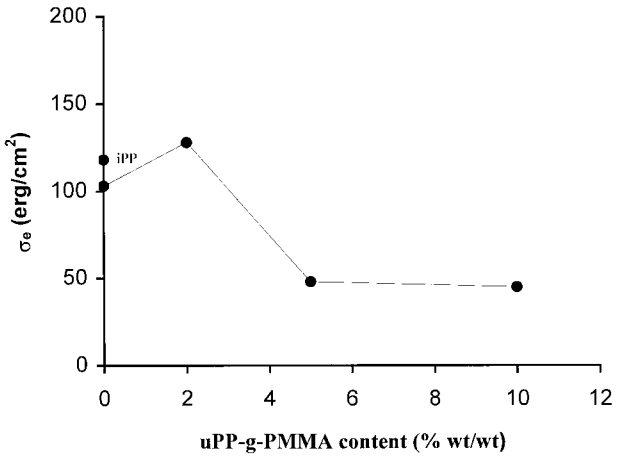

Figure 11 Plots of the surface free energy of folding (σ_e) of lamellar crystals of iPP phase as a function of uPP-*g*-PMMA content (wt/wt).

Figure 12 Schematic models of the lamellar structure of iPP phase crystallized under controlled undercooling from melts of plain iPP and iPP/aPMMA/uPP-*g*-PMMA blends.

the plain iPP according to the schematic models reported in Figure 12.

Work is in progress to investigate the influence of the crystallization conditions on morphology and thermal behavior of the samples of binary aPMMA/uPP-*g*-PMMA and of iPP/uPP-*g*-PMMA blends isothermally crystallized in the same T_c range of the iPP phase.

CONCLUSIONS

Samples of blends of iPP and aPMMA isothermally crystallized at temperatures of 126, 130, 134, and 138°C exhibit a coarse morphology of the aPMMA phase in which domains are occluded in the iPP intra- and interspherulitic contact regions. For comparatively higher undercooling, owing to the relatively high rate of the iPP crystallization at the examined T_c, the crystallization process of the iPP phase freezes the melt morphology of the aPMMA phase. With reducing undercooling, the dispersion coarseness of the aPMMA domains increases, suggesting that during the iPP crystallization process, a coalescence phenomenon is undergone by the primary particles formed in the melt state. Moreover, for a given T_c, an average crystalline thickness and interlamellar amorphous layer comparable to that developed in the plain iPP characterize the lamellar crystals in the iPP spherulites fibrillae. The addition of uPP-*g*-PMMA copolymer is found to affect the interfacial tension between iPP and aPMMA phases in the melt state; the observed changes in the aPMMA particle size and particle size distribution depending on composition. After complete crystallization of the iPP phase at temperatures of 126, 130, 134, and 138°C, the pres-

ence of the uPP-*g*-PMMA phase modifies not only mode and state of dispersion of minor component, but also iPP spherulitic texture and inner structure of spherulites fibrillae. The extent of the induced modifications, i.e., the degree of compatibilization achieved, depends on a combination of composition and undercooling. For high undercooling, comparatively higher homogeneous texture and finer dispersion coarseness is shown by the material containing 5% of uPP-*g*-PMMA copolymer. For low undercooling, the blend spherulitic texture, rather than the mode and state of dispersion of minor component, is modified deeply. Amorphous interspherulitic contact regions, whose number per unit area increases with increasing uPP-*g*-PMMA content, are observed. Moreover, the phase structure generated in iPP/aPMMA/uPP-*g*-PMMA materials is characterized by an average crystalline lamellar thickness (L_c) and amorphous interlayer, comparable to that shown by the plain iPP for low uPP-*g*-PMMA amount, whereas considerably lower L_c values by increasing copolymer content are found. Also, relevant thermodynamic parameters of the iPP phase are strongly modified by the presence of the uPP-*g*-PS phase; opposite effects are observed depending on composition. The values of both the equilibrium melting temperature (T_m) and of the surface free energy of folding (σ_e) of the iPP lamellar crystals are in fact found, for low and high uPP-*g*- PMMA content, to be higher and lower respectively than that shown by the plain iPP. Such T_m and σ_e values of iPP phase have been ascribed to the growth of lamellar crystals with different perfection and/or thickness and surface disorder probably related to the phase nature and concentration in the immediate regions of the growing lamellae. In particular, miscibility effects between uPP-*g*-PMMA propylenic sequences and iPP have been hypothesized to affect the constitutional and conformational regularity of crystallizable iPP chains.

REFERENCES

1. D'Orazio, L.; Guarino, R.; Mancarella, C.; Martuscelli, E.; J Appl Polym Sci 1997, 66, 2377.
2. Cecchin, G.; Guglielmi, F.; Zerega, F. U. S. Pat. 4,602,077, 1986.
3. Cecchin, G.; De Nicola, A. U. S. Pat. 5,159,023, 1990.
4. Brandrup, S.; Immergut, E. M. Polymer Handbook; Interscience: New York, 1975; Vol. 5.
5. Vonk, C. G. J Appl Crystallogr 1975, 8, 340.
6. Alexander, L. E. X-Ray Diffraction in Polymer Science; Wiley: New York, 1969.
7. Turnbull, D.; Fisher, J. C., J Chem Phys 1949, 17, 71.
8. Bartczak, Z.; Galeski, A.; Martuscelli, E. Polym Eng Sci 1984, 24, 1155.
9. Hoffman, J. D.; Miller, R. L. Polymer 1997, 38, 3151.